Vibrationally Resolved Inner-Shell Photoexcitation of the Molecular Anion C_2^-

S. Schippers,*[a] P.-M. Hillenbrand+,[a] A. Perry-Sassmannshausen+,[a] T. Buhr+,[a] S. Fuchs+,[a] S. Reinwardt+,[b] F. Trinter+,[c] A. Müller+,[a] and M. Martins+[b]

Carbon 1s core-hole excitation of the molecular anion C_2^- has been experimentally studied at high resolution by employing the photon-ion merged-beams technique at a synchrotron light source. The experimental cross section for photo–double-detachment shows a pronounced vibrational structure associated with $1\sigma_u \rightarrow 3\sigma_g$ and $1\sigma_g \rightarrow 1\pi_u$ core excitations of the C_2^- ground level and first excited level, respectively. A detailed Franck-Condon analysis reveals a strong contraction of the C_2^- molecular anion by 0.2 Å upon this core photoexcitation. The associated change of the molecule's moment of inertia leads to a noticeable rotational broadening of the observed vibrational spectral features. This broadening is accounted for in the present analysis which provides the spectroscopic parameters of the C_2^- $1\sigma_u^{-1} 3\sigma_g^2\ ^2\Sigma_u^+$ and $1\sigma_g^{-1} 3\sigma_g^2\ ^2\Sigma_g^+$ core-excited levels.

Introduction

With the advent of third-generation synchrotron light sources and x-ray free-electron lasers, inner-shell ionization of free molecules has become a topic of intense experimental research.[1–7] Using *neutral molecules* as targets, many fundamental questions have been addressed in recent years, e.g., the localization of the core hole,[8] complex many-electron relaxation effects,[9–12] or the role of the photon momentum in the molecular dissociation process.[13,14] *Molecular ions* have received much less attention despite their important role as transient species in many chemical environments such as flames,[15] Earth's and Titan's ionospheres,[16,17] or interstellar gas clouds.[18,19] This is due to the fact that only much lower target densities can be prepared for targets of free charged particles as compared to what can be achieved for neutral species. Nevertheless, recent progress in ion-beam and ion-trap techniques has lead to first precision inner-shell studies with *positively* charged molecular ions.[20–30]

Here, we report on 1s inner-shell photoexcitation of the *negatively* charged molecular ion C_2^-. Much experimental work on C_2^- has addressed the valence shell using a number of spectroscopic techniques.[31–39] Recently, C_2^- has been identified as a promising molecular species for laser cooling,[40] and the corresponding transitions have been studied with high precision.[41] In the present study, we have measured relative cross sections for 1s inner-shell photo–double-detachment (PDD) of C_2^- anions, i.e., for the process

$$h\nu + C_2^- \rightarrow C_2^+ + 2e^-. \tag{1}$$
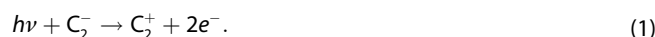
We used a sufficiently high photon-energy resolving power that allowed us to resolve transitions between individual vibrational levels, thus, providing detailed insight into the highly correlated nuclear and electronic relaxation dynamics, which sets in after the initial creation of a C 1s core hole. Previous work on inner-shell photoabsorption by molecular anions was either confined to inner-valence shells[42,43] or, for photoabsorption by K-shell electrons, used rather low photon-energy resolving powers.[44,45]

[a] Prof. Dr. S. Schippers, Dr. P.-M. Hillenbrand,+ Dr. A. Perry-Sassmannshausen,+ Dr. T. Buhr,+ S. Fuchs,+ Prof. Dr. A. Müller+
I. Physikalisches Institut, Justus-Liebig-Universität Gießen, Heinrich-Buff-Ring 16, 35392 Giessen, Germany
E-mail: stefan.schippers@physik.uni-giessen.de
Homepage: http://www.uni-giessen.de/amp

[b] S. Reinwardt,+ Dr. M. Martins+
Institut für Experimentalphysik, Universität Hamburg, Luruper Chaussee 149, 22761 Hamburg, Germany

[c] Dr. F. Trinter+
Institut für Kernphysik, Goethe-Universität Frankfurt am Main, Max-von-Laue-Straße 1, 60438 Frankfurt am Main, Germany
and
Molecular Physics, Fritz-Haber-Institut der Max-Planck-Gesellschaft, Faradayweg 4–6, 14195 Berlin, Germany

[+] These authors contributed equally.

An invited contribution to a Special Collection on Synchrotron-Based Photo- and Physical Chemistry

Experimental Setup

The present experiment was performed at the photon-ion merged-beams setup PIPE,[46–48] a permanently installed end-station at the photon beamline P04[49] of the PETRA III synchrotron light source, operated by DESY in Hamburg, Germany. Using the same procedures as in a previous experiment with atomic C⁻ anions,[50] a C_2^- ion beam was generated with a Cs-sputter ion source, accelerated to a kinetic energy of 6 keV, and magnetically analyzed for isolating ions with the desired mass-over-charge ratio. Subsequently, the mass-over-charge-selected $^{12}C^{12}C^-$ ion beam was collimated and electrostatically deflected such that it moved coaxially with the counter-propagating photons over a distance of ~1.7 m length. The collimated C_2^- ion current in the photon-ion interaction region amounted to typically 10 nA, and the photon flux was 9×10^{11} s⁻¹ at a photon energy of 280 eV and a photon-energy spread of 500 meV. This rather low photon flux at the

ChemPhysChem

Research Article
doi.org/10.1002/cphc.202300061

**Chemistry
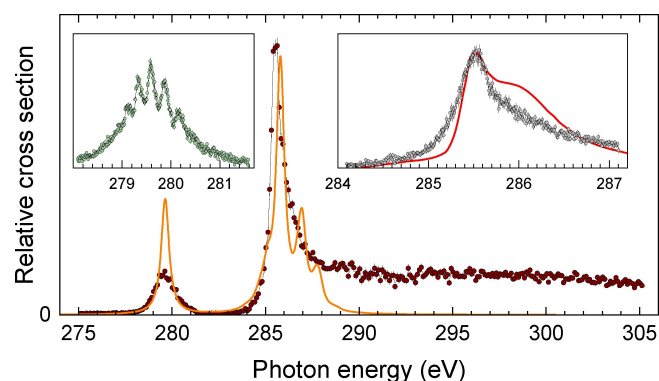Europe**
European Chemical
Societies Publishing

photon energies of present interest resulted from strong photo-absorption by carbon contaminations on the surfaces of the photon beamline's optical components.

The photon-energy scale was calibrated by performing photo-absorption measurements in N_2 and Ne gases and by linearly scaling the photon energy such that the positions of the measured absorption resonance features matched known energies.[47,51,52] An additional energy correction accounted for the Doppler shift associated with the directed movement of the ions in the primary C_2^- ion beam relative to the photon beam. The resulting uncertainty of the present calibrated energy scale amounts to ±0.2 eV.

The elongated photon-ion interaction volume ensured that the number of photoionization events was sufficiently large for acquiring an acceptably low level of statistical uncertainty in a reasonable amount of time despite the diluteness of the ionic target. Behind the photon-ion interaction region, the C_2^+ reaction products were magnetically separated from the C_2^- primary ion beam and directed onto a single-particle detector. Background resulting from charge-changing collisions with residual-gas particles was determined by separate measurements in absence of the photon beam. At the maximum of the first resonance in Figure 1, the signal count rates amounted to about 1 kHz and 150 Hz at photon-energy spreads of 500 meV and 50 meV, respectively. The background count rate was about 10 Hz in both cases. The background-subtracted photo-product count rate was normalized to the primary ion current, which was continuously measured with a Faraday cup, and to the photon flux, that was monitored by a calibrated photodiode. This procedure resulted in the relative cross sections for PDD of C_2^- anions that are displayed in Figure 1.

Results and Discussion

The main panel of Figure 1 provides an overview over the PDD cross section in the vicinity of the C_2^- 1σ ionization threshold which has been theoretically predicted at 284.1 eV.[45] The cross section exhibits two resonance features, one ~4.5 eV below this threshold and one ~1.4 eV above. These two features were already observed in the experimental data communicated by Berrah and Bilodeau to Douguet et al.[45] These data were measured at a similar photon-energy spread as in the present overview scan. To obtain more accurate information about the resonance features, we have measured both features also at a lower photon-energy spread of approximately 50 meV. This reveals the vibrational structure of the first resonance (left inset of Figure 1). However, no such vibrational structure is discernible for the second resonance (right inset of Figure 1).

The main panel of Figure 1 also displays a theoretical cross section for photoabsorption of C_2^-. It was calculated with the ORCA quantum chemistry program package[53] (version 5.0.3) using the def2-TZVPP[54] and def2/J[55] basis sets as well as 20 uncontracted Gaussian s- and p-type functions[56] for a better description of the Rydberg states. In the TDDFT calculations, the CAM-B3LYP[57] functional was employed together with the RIJCOSX[58] approximation for the evaluation of matrix elements. For the comparison with the experimental data the calculated cross section was convolved with a Gaussian with a full width at half maximum (FWHM) of 0.5 eV, multiplied with a constant factor, and shifted by 10.5 eV towards higher energies.

Before discussing the comparison between experiment and theory, it should be recalled that the measured double detachment cross section does not directly correspond to the calculated absorption cross section. Next to double detachment, other processes do contribute to photoabsorption as well such as single detachment or molecular breakup into neutral or charged atomic fragments. Generally, the branching ratios for the various final channels depend on the photon energy. For example, above the threshold for direct C 1s detachment, net single detachment becomes improbable since the C K-shell hole that is formed by the primary detachment process will be most probably filled by an Auger process leading either to double detachment where the molecule is left intact (this is what has been observed in the present experiment) or to fragmentation.

As for the present ORCA calculation, there is agreement between experiment and theory concerning the energy separation between the two experimentally observed resonance features (Figure 1). The calculated relative strengths of these two features agree less with the experimental findings. This may be attributed to different double-detachment branching ratios for both resonance features. Moreover, the ion beam probably contained a sizeable fraction of metastable C_2^- anions (see below) whereas, in the calculation, it was assumed that all ions were in their ground level. The asymmetric shape of the above-threshold resonance is explained by the presence of multiple resonances of decreasing strength with increasing energy. However, in the experimental cross section, this resonance structure is more smeared out than predicted by theory. The theoretical calculation does not account for direct ionization of a C 1s electron which dominates the experimental cross section above about 288 eV.

The cross section for C_2^- photodetachment has been calculated previously by Douguet et al.[45] who considered only

Figure 1. Experimental cross sections (symbols) for PDD of C_2^-. The main panel provides an overview over the entire experimental photon-energy range which was scanned at a photon-energy spread of $\Delta E_{exp} \approx 500$ meV. The orange full line is the theoretical absorption cross section calculated within this work (see text), scaled and shifted in energy (by +10.5 eV) to match the experiment. The insets display high-resolution measurements ($\Delta E_{exp} \approx 50$ meV) of the resonance features. In all cases, the statistical error bars represent one standard deviation. All cross section scales are linear. The red full line in the right inset is the theoretical cross section for photodetachment of C_2^- by Douguet et al.,[45] scaled to the experimental cross section and shifted by −0.1 eV.

ChemPhysChem

Research Article
doi.org/10.1002/cphc.202300061

Chemistry
Europe
European Chemical
Societies Publishing

the strong above-threshold resonance. The red full line in the right inset of Figure 1 displays their result, scaled to the present experimental cross section and shifted by -0.1 eV on the photon-energy axis. This shift is within the present ±0.2 eV experimental uncertainty. While experiment and theory agree about the position of this resonance feature, there are slight differences concerning its shape, in particular, on the high-energy side of the peak where the theoretical calculation predicts a pronounced shoulder, which is not present in the experimental data. However, one again has to take note of the fact that different final channels were considered in theory (single detachment) and experiment (double detachment). According to the calculations, the resonance classifies as a shape resonance associated with $1\sigma_g \rightarrow k\pi_u$ dipole excitations to short-lived levels of $^2\Pi_u$ symmetry. These are weakly bound in a shallow potential supporting only a few narrowly spaced vibrational levels, which cannot be resolved even by our high-resolution measurement.

The lowest 1σ core excitation of the C_2^- $1\sigma_g^2 1\sigma_u^2 2\sigma_g^2 2\sigma_u^2 1\pi_u^4 3\sigma_g\, X\,^2\Sigma_g^+$ ground level is a $1\sigma_u \rightarrow 3\sigma_g$ excitation to the $1\sigma_u^{-1} 3\sigma_g^2\,^2\Sigma_u^+$ level. Corresponding vibrationally resolved photoabsorption resonances were observed for iso-electronic N_2^+.[25] Therefore, we assign the vibrationally resolved C_2^- resonance structure to the same electronic transition, despite of the fact that the vibrational structure of the positive ion differs significantly from the present one for the negatively charged carbon dimer. For N_2^+, the strongest vibrational transition is associated with the $v' = 0$ excited vibrational level and the contributions by higher vibrational levels decrease monotonically with increasing vibrational quantum number v' such that individual peaks can only be discerned for $v' = 0$, $v' = 1$, and $v' = 2$. For C_2^-, the vibrational distribution is much broader attaining its maximum at $v' = 5$ (Figure 2). This behavior is related to a substantial change of the C_2^- bond length upon $1\sigma_u \rightarrow 3\sigma_g$ core excitation as revealed by the Franck-Condon analysis that is discussed in the following.

Franck-Condon Analysis

Our Franck-Condon analysis consists of fitting a sum of Voigt line profiles $V(E, \Delta E_{exp}, \gamma, E_{vv'}, f_{vv'})$ to our experimental high-resolution data with each profile representing a transition between a vibrational level v of the initial electronic level and a vibrational level v' of the core-excited potential curve. The Voigt profiles are functions of the photon energy E. Their widths are characterized by the experimental photon-energy spread $\Delta E_{exp} = 0.05$ eV (Gaussian full width at half maximum) and by the Lorentzian width γ that is associated with the core-hole lifetime of the core-excited level. In principle, the Lorentzian width should also depend on v and v'. However, the present data do not suggest that there is a noticeable dependence of γ on the vibrational quantum numbers. Therefore, it is not taken into account in our present analysis. The individual Voigt profiles are centered at the vibrational transition energies $E_{vv'}$. The relative strengths of the transitions are given by the corresponding Franck-Condon factors $f_{vv'}$ which are calculated
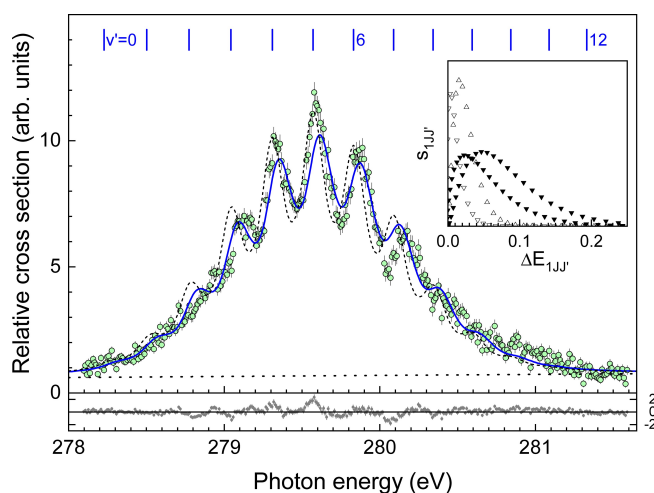
Figure 2. Experimental cross section for PDD of C_2^- (symbols with statistical error bars representing one standard deviation) and the fit (blue full curve) of Equations 2 and 3 with $k_{max} = 1$, $v_{max} = 1$, and $v'_{max} = 12$ for only the $1\sigma_u \rightarrow 3\sigma_g$ core excitation of the $X\,^2\Sigma_g^+$ ground level. The dotted line represents the continuum cross section for L-shell detachment as obtained from the fit. The vertical bars mark the vibrational energies for $v = 0 \rightarrow v'$ transitions that result from the fit. The dashed curve is obtained if the rotational temperature is set to zero and all other fit parameters remain unchanged. It allows one to assess the influence of rotational broadening on the shape of the spectrum. The inset shows the underlying rotational energy (Equation 4) distributions for the $J \rightarrow J' = J + 1$ (triangles up) and $J \rightarrow J' = J - 1$ (triangles down) transitions with even J between the lower $X\,^2\Sigma_g^+$ and the upper $^2\Sigma_u^+$ C_2^- rotational levels for the temperatures $T = 1100$ K (full symbols) as used in the fit and $T = 300$ K for comparison (open symbols). Odd J values and $J \rightarrow J' = J$ transitions do not occur because of nuclear-spin statistics. The lower panel displays the residuals of the fit together with the experimental error bars. The reduced χ^2 of the fit is 3.19.

from the potential parameters of the lower and upper potential curves (Morse potentials).

Concretely, the fit function in the present Franck-Condon analysis was

$$\sigma(E) = b_0 + b_1 E + \sum_{k=1}^{k_{max}} S_k \sigma_k(E) \tag{2}$$

where the coefficients b_0 and b_1 account for the continuum cross section for L-shell detachment and the sum extends over different electronic transitions enumerated by the summation index k, and the factors S_k denote the associated apparent (relative) transition strengths. Each individual electronic transition k contributes to the absorption cross section

$$\sigma_k(E) = \sum_{v=0}^{v_{max}} n_{kv} \sum_{v'=0}^{v'_{max}} \sum_{J=0}^{J_{max}} \sum_{J'=J-1}^{J+1} s_{kJJ'} \times$$
$$V(E, \Delta E_{exp}, \gamma_k, E_{kvv'} + \Delta E_{kJJ'}, f_{kvv'}), \tag{3}$$

with n_{kv} denoting the fractional populations of the initial vibrational level v of the electronic transition k. The sum over the rotational quantum numbers J and J' and the quantities $s_{kJJ'}$

ChemPhysChem

Research Article
doi.org/10.1002/cphc.202300061

**Chemistry
Europe**
European Chemical
Societies Publishing

and $\Delta E_{kJJ'}$ account for rotational broadening as detailed below. The calculation of the Franck-Condon factors between two displaced Morse potentials follows the prescription of López et al.[59] It involves a numerical integration which is carried out by using an adaptive Gauss-Kronrod algorithm and extended precision arithmetic as implemented in the boost C^{++} libraries.[60] We verified the accuracy of our numerical integration procedure by reproducing the Franck-Condon factors tabulated by López et al.[59]

In the fits below, the parameters b_0, b_1, S_k from Equation 2, γ_k from Equation 3, as well as the parameters $\hbar\omega_e$, $\hbar\omega_e\chi_e$, and R_e of the core-excited Morse potential curves[59] were varied simultaneously. In each fit step, the momentary values of the Morse parameters were used for the calculation of the vibrational energies $E_{kvv'}$ and the Franck-Condon factors $f_{kvv'}$ appearing in Equation 3. An additional free fit parameter was the temperature pertaining to the vibrational and rotational degrees of freedom. This temperature determined the values of n_{kv} and $s_{kJJ'}$ from Equation 3 as explained below.

Fit Considering One Electronic Transition

In a first fit, only the $1\sigma_u \rightarrow 3\sigma_g$ transition from the $X\,^2\Sigma_g^+$ electronic ground level was considered. The potential parameters of this level were taken from recent theoretical work,[61] where excellent agreement with the available experimental data[33,34] was achieved. The potential parameters of the core-excited potential curve were varied in the fit. This fit result is displayed in Figure 2. It reproduces the overall resonance structure, albeit not in every detail. Nevertheless, the fit reveals that the maximum vibrational transition strength occurs for the $v = 0 \rightarrow v' = 5$ transition and that this is related to a strong decrease of the C_2^- bond length by almost -0.2 Å upon $1\sigma_u \rightarrow 3\sigma_g$ core excitation. For isoelectronic N_2^+, the corresponding decrease was found to be only -0.04 Å,[25] leading to a drastically different vibrational resonance structure as compared to C_2^-.

The large change of the C_2^- bond length upon inner-shell excitation entails a large change of the molecule's moment of inertia. This and the high molecular temperature of ~ 1100 K (see below) leads to a noticeable rotational broadening of the vibrational spectral structures. This effect was not considered in the analysis of the vibrationally resolved inner-shell detachment of N_2^+,[25] where the photo-induced change of bond length was found to be comparatively moderate and where the molecular ions were internally colder. In our fit, we have quantified the rotational broadening within the rigid-rotator approximation. Accordingly, the rotational constant B_e scales with R_e^{-2}. With $\Delta R_e = -0.2$ Å, the rotational constant $B_e' = B_e[R_e/(R_e + \Delta R_e)]^2$ of the upper $^2\Sigma_u^+$ level is larger than B_e of the $X\,^2\Sigma_g^+$ ground level by more than 40%. The associated change of the C_2^- rotational energy upon 1s core excitation depends on the rotational quantum numbers J and J' of the lower and upper levels, respectively. It amounts to

$$\Delta E_{JJ'} = hc[B_e'J'(J'+1) - B_eJ(J+1)]. \qquad (4)$$

Assuming a Boltzmann distribution for the rotational levels of the $X\,^2\Sigma_g$ electronic ground level and accounting for nuclear-spin statistics[62] as well as for the relative rotational transition strengths (Hönl-London factors[63] denoted as $s_{kJJ'}$ in Equation 3), one arrives at the rotational-energy distributions that are shown in the inset of Figure 2. The distribution for a temperature of 1100 K is strongly asymmetric. The mean energy shift amounts to 54.2 meV and its standard deviation to 3.2 meV, thus, leading to a significant shift and broadening of the vibrational resonances as can be seen from a comparison of the fit curve with the dashed curve in Figure 2 which was calculated from the same set of fit parameters but does not account for rotational effects.

Fit Considering Two Electronic Transitions

The agreement between fitted and experimental curve in Figure 2 is not satisfying. An attempt to include nonthermal populations of higher initial vibrational levels resulted in a smearing out of the vibrational resonance structures and was not pursued any further. Instead, we considered a second electronic transition starting from the first electronically excited level $1\sigma_g^2 1\sigma_u^2 2\sigma_g^2 2\sigma_u^2 1\pi_u^3 3\sigma_g\,A\,^2\Pi_u$. In the Cs-sputter source, C_2^- anions are formed, when the carbon particles sputtered from the cathode traverse the Cs monolayer covering the cathode. The electron transfer of Cs valence electrons to the C_2 dimers generates C_2^- anions in the electronic ground state as well as in electronically excited states.[36] The $A\,^2\Pi_u$ level has an excitation energy of ~ 0.5 eV and lifetimes of 50 μs for $v = 0$ and 40 μs for $v = 1$.[61,64] These lifetimes are of the order of the flight time of the ions from the ion source to the merged-beams interaction region. Therefore, it must be expected that a fraction of the C_2^- anions is in this metastable electronically excited level. The second electronically excited level of C_2^-, the $B\,^2\Sigma_u^+$ level with an excitation energy of ~ 2.3 eV, has a lifetime of less than 80 ns[31,61,64] which is much shorter than the ions' flight time. Therefore, this level was not taken into account in the present analysis.

The lowest core-excitation channel of the $A\,^2\Pi_u$ level is the $1\sigma_g \rightarrow 1\pi_u$ transition to the $1\sigma_g^{-1} 1\sigma_u^2 2\sigma_g^2 2\sigma_u^2 1\pi_u^4 3\sigma_g\,^2\Sigma_g^+$ level. Inclusion of both the $1\sigma_u \rightarrow 3\sigma_g$ and $1\sigma_g \rightarrow 1\pi_u$ transitions from the $X\,^2\Sigma_g^+$ and $A\,^2\Pi_u$ levels to the nearly degenerate $1\sigma_u^{-1} 3\sigma_g^2\,^2\Sigma_u^+$ and $1\sigma_g^{-1} 3\sigma_g^2\,^2\Sigma_g^+$ levels, respectively, resulted in the much improved fit displayed in Figure 3. The potential parameters that were determined by this fit are provided in Table 1 and the respective Frank-Condon factors $f_{kvv'}$ (Equation 3) are plotted in Figure 4.

The fit suggests that the contribution of the $A\,^2\Pi_u$ level to the PDD cross section is substantial ($55 \pm 7\%$). It should be kept in mind that this percentage does not correspond to the initial population of this level. It also reflects the relative line strength of the core-exciting $1\sigma_g \rightarrow 1\pi_u$ transition which might be larger
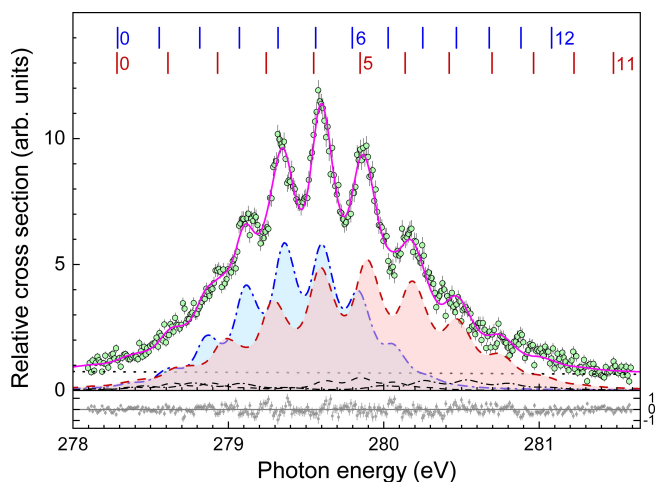
Figure 3. Experimental cross section for PDD of C_2^- (symbols with statistical error bars representing one standard deviation) and the fit (pink full curve) of Equations 2 and 3 with $v_{max} = 1$ and $v'_{max} = 12$ for two electronic transitions ($k_{max} = 2$). The blue dashed-dotted and red dashed shaded curves represent $S_k \sigma_k(E)$ for $k = 1$ and $k = 2$, respectively. The dash-dotted and dashed thin black lines are the respective contributions by the $v = 1$ initial vibrational level. The dotted line represents the continuum cross section for L-shell detachment as obtained from the fit. The vertical bars mark the vibrational energies $E_{k0v'}$ with the upper (lower) row corresponding to $k = 1$ ($k = 2$). They are labelled by the vibrational quantum number v' of the excited electronic level. The lower panel displays the residuals of the fit together with the experimental error bars. The reduced χ^2 of the fit is 1.80.

than the one of the $1\sigma_u \rightarrow 3\sigma_g$ transition from the $X\,^2\Sigma_g^+$ ground level.

Figure 5 displays the Morse potentials that correspond to the D and β values from Table 1. The contraction of the molecule upon 1σ core excitation is obvious. The minima of the core-excited potential curves are shifted by -0.19 and -0.20 Å, respectively, to considerably lower internuclear distances as compared to the $X\,^2\Sigma_g^+$ and $A\,^2\Pi_u$ potentials. These changes in bond length are considerably larger than what has been reported for isoelectronic N_2^+, where the respective value for the core excitation of the $X\,^2\Sigma_g^+$ ground level is -0.04 Å.[25] The difference of 0.15 Å between $\varDelta R_e$ for the core excitation of the C_2^- and N_2^+ $X\,^2\Sigma_g^+$ levels stems exclusively from the difference in the $X\,^2\Sigma_g^+$ equilibrium bond lengths which are 1.27 and 1.12 Å, respectively. Notably, the bond length of 1.08 Å of the core-excited $^2\Sigma_u^+$ level is the same for both molecular species,

i.e., upon core photoexcitation, C_2^- seems to lose its anionic character.

It is somewhat surprising that the potential curves of the two core-excited $1\sigma_{u/g}^{-1} 3\sigma_g\,^2\Sigma_{u/g}^+$ levels should be different since one would expect a near degeneracy. It should, however, be noted that the differences between the Morse parameters D and β for both levels are within their mutual fit uncertainties (Table 1). We also tried a fit where we imposed the additional constraint that $\hbar\omega_e$, $\hbar\omega_e\chi_e$, and R_e be the same for both core-excited levels. The result of this fit was not much different from the fit curve in Figure 2, i.e., some difference between the two core-excited potential curves seems to be a requirement for an improved fit.

In the fit, the rotational broadening was accounted for as discussed above. The resulting rotational temperature of 1095 ± 137 K corresponds roughly to the expected temperature of the cesium vapor in our Cs-sputter ion source. Moreover, it was assumed that the same temperature also determines the populations of the $X\,^2\Sigma_g^+$ and $A\,^2\Pi_u$ vibrational levels. Accordingly, the relative populations n_{kv} (Equation 3) of the $X\,^2\Sigma_g^+ (A\,^2\Pi_u)$ $v = 0$ and $v = 1$ levels were 91% (90%) and 9% (10%), respectively. Within this approach, the initial populations of all higher vibrational levels were insignificant. As already mentioned above, larger contributions from higher vibrational levels would smear out the observed vibrational resonance structures and, thus, be at odds with the experimental observation.

In addition to the rotational broadening, also the lifetime broadening was obtained from the fit. The present lifetime widths of 124(12) meV and 154(21) meV (Table 1) are reasonably close to the more exact values for other carbon-containing small molecules such as, e.g., 99(2) meV for CO_2[65] and 100(1) meV for C_2H_2.[66] In all fits, the instrumental width was kept fixed at its nominal value $\Delta E = 50$ meV.

Conclusions

Using the photon-ion merged-beams technique, we have measured inner-shell photoabsorption of a molecular anion. The experimental approach is quite general and will be further exploited for investigating the interaction of energetic radiation with reactive molecular species. The favorable conditions with respect to photon flux and resolving power at beamline P04 of the PETRA III synchrotron light source enabled us to resolve

Table 1. Spectroscopic parameters resulting from the fit of Equations 2 and 3 to the experimental data displayed in Figure 3, i.e., the minimum T_e of the potential curve, the harmonic frequency ω_e, the anharmonicity coefficient $\omega_e\chi_e$, the equilibrium bond length R_e, and the natural line width γ. The depths and the inverse ranges of the Morse potentials were calculated as $D = \hbar\omega_e^2/(4\omega_e\chi_e)$ and $\beta = (2\mu\omega_e\chi_e/\hbar)^{1/2}$.[59] In the latter expression, μ denotes the reduced mass. Also given are the rotational constants B_e and the differences ΔR_e between the bond lengths of the lower and upper levels. The parameters for the $X\,^2\Sigma_g$ ground level and the $A\,^2\Pi_u$ metastable level were taken from [61]. Numbers in parentheses signify the (uncorrelated) errors from the fit. In addition, T_e is subject to the systematic experimental uncertainty of the energy calibration of ± 0.2 eV.

k	Level	T_e [eV]	$\hbar\omega_e$ [meV]	$\hbar\omega_e\chi_e$ [meV]	D [eV]	β [Å^{-1}]	B_e [cm^{-1}]	R_e [Å]	ΔR_e [Å]	γ [meV]
1	$(1\pi_u^4\, 3\sigma_g)\, X\,^2\Sigma^+$	0.0	220.84	1.4289	8.5330	2.0253	1.7438	1.2689	–	
1	$1\sigma_u^{-1}\, 1\pi_u^4\, 3\sigma_g^2\,^2\Sigma^+$	278.26(2)	274(8)	3.2(6)	5.9(12)	3.0(3)	2.42(1)	1.077(2)	$-0.191(2)$	124(12)
2	$(1\pi_u^3\, 3\sigma_g^2)\, A\,^2\Pi_u$	0.49655	206.90	1.3387	7.9939	1.9604	1.6424	1.3075	–	
2	$1\sigma_g^{-1}\, 1\pi_u^4\, 3\sigma_g^2\,^2\Sigma^+$	278.38(3)	342(6)	3.7(5)	7.9(14)	3.3(3)	2.30(2)	1.105(4)	$-0.202(4)$	154(21)
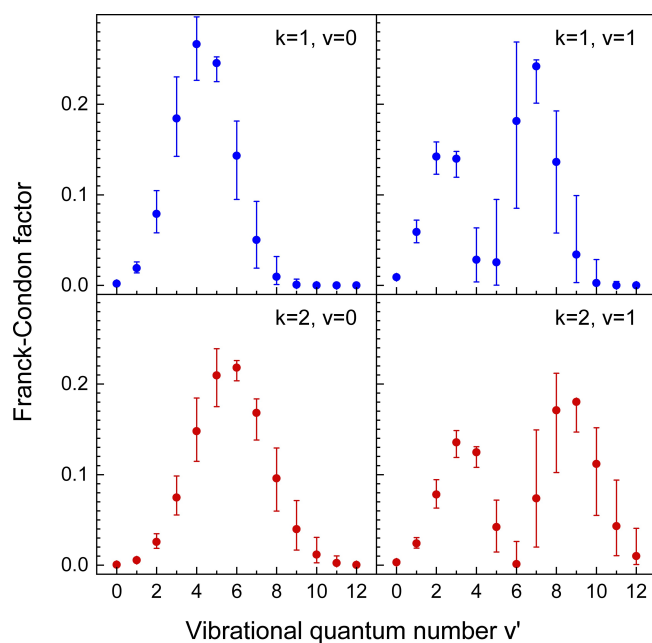
Figure 4. Franck-Condon factors $f_{kvv'}$ resulting from the fit of Equations 2 and 3 to the experimental data (Figure 3). The vibrational quantum numbers v and v' refer to the lower and upper levels, respectively, of the electronic transitions k. The error bars were obtained from varying uncorrelatedly the parameters R_e, $\hbar\omega_e$, and $\hbar\omega_e\chi_e$ of the upper levels within the respective uncertainty intervals from Table 1.
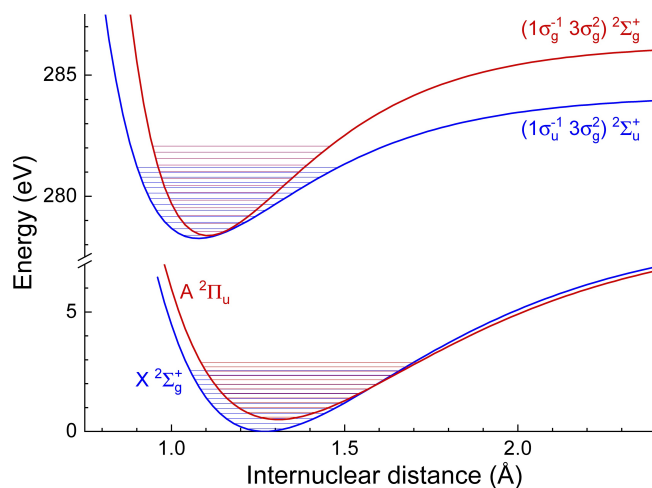
Figure 5. Morse potentials with their 12 lowest vibrational levels resulting from the spectroscopic parameters given in Table 1.

individual vibrational transitions to core-excited C_2^- molecular levels and to extract their potential parameters from a detailed Franck-Condon analysis, which consistently accounts for vibrational and rotational effects. This analysis revealed that the dicarbon anion shrinks substantially by 0.2 Å upon 1σ core excitation. Similarly strong geometrical changes might also be expected for the photoexcitation of other anionic molecular systems.

The present results may aid the detection of C_2^- in cold cosmic gas clouds where several hydrogenated C_nH^- species have been identified owing to their large dipole moments.[19] So far, the infrared-inactive C_2^- anion has not been discovered in space. The presently measured C_2^- double-detachment cross section exhibits clear spectral signatures in the soft x-ray spectral range which can help to identify interstellar C_2^- by upcoming high-resolution x-ray telescopes such as Athena.[67] We also hope that the present work stimulates the further development of the theoretical tools (see, e.g., Huang et al.[68]) for a more exact treatment of core-excited molecules.

Conflict of Interest

The authors do not declare any conflict of interest.

Data Availability Statement

The data that support the findings of this study are available from the corresponding author upon reasonable request.

[1] K. Ueda, *J. Phys. B* **2003**, *36*, R1.
[2] U. Hergenhahn, *J. Phys. B* **2004**, *37*, R89.
[3] R. Feifel, M. N. Piancastelli, *J. Electron Spectrosc. Relat. Phenom.* **2011**, *183*, 10.
[4] C. Miron, P. Morin, High-resolution inner-shell photoionization, photoelectron and coincidence spectroscopy, in M. Quack, F. Merkt (Editors), *Handbook of High-resolution Spectroscopy*, pages 1655–1689, John Wiley & Sons, Ltd. **2011**.
[5] L. Young, K. Ueda, M. Gühr, P. H. Bucksbaum, M. Simon, S. Mukamel, N. Rohringer, K. C. Prince, C. Masciovecchio, M. Meyer, A. Rudenko, D. Rolles, C. Bostedt, M. Fuchs, D. A. Reis, R. Santra, H. Kapteyn, M. Murnane, H. Ibrahim, F. Légaré, M. Vrakking, M. Isinger, D. Kroon, M. Gisselbrecht, A. L'Huillier, H. J. Wörner, S. R. Leone, *J. Phys. B* **2018**, *51*, 032003.

[6] K. Ueda, E. Sokell, S. Schippers, F. Aumayr, H. Sadeghpour, J. Burgdörfer, C. Lemell, X.-M. Tong, T. Pfeifer, F. Calegari, A. Palacios, F. Martin, P. Corkum, G. Sansone, E. V. Gryzlova, A. N. Grum-Grzhimailo, M. N. Piancastelli, P. M. Weber, T. Steinle, K. Amini, J. Biegert, N. Berrah, E. Kukk, R. Santra, A. Müller, D. Dowek, R. R. Lucchese, C. W. McCurdy, P. Bolognesi, L. Avaldi, T. Jahnke, M. S. Schöffler, R. Dörner, Y. Mairesse, L. Nahon, O. Smirnova, T. Schlathölter, E. E. B. Campbell, J.-M. Rost, M. Meyer, K. A. Tanaka, *J. Phys. B* **2019**, *52*, 171001.

[7] M. N. Piancastelli, T. Marchenko, R. Guillemin, L. Journel, O. Travnikova, I. Ismail, M. Simon, *Rep. Prog. Phys.* **2020**, *83*, 016401.

[8] M. S. Schöffler, J. Titze, N. Petridis, T. Jahnke, K. Cole, L. P. H. Schmidt, A. Czasch, D. Akoury, O. Jagutzki, J. B. Williams, N. A. Cherepkov, S. K. Semenov, C. W. McCurdy, T. N. Rescigno, C. L. Cocke, T. Osipov, S. Lee, M. H. Prior, A. Belkacem, A. L. Landers, H. Schmidt-Böcking, T. Weber, R. Dörner, *Science* **2008**, *320*, 920.

[9] T. Jahnke, A. Czasch, M. Schöffler, S. Schössler, M. Käsz, J. Titze, K. Kreidi, R. E. Grisenti, A. Staudte, O. Jagutzki, L. P. H. Schmidt, T. Weber, H. Schmidt-Böcking, K. Ueda, R. Dörner, *Phys. Rev. Lett.* **2007**, *99*, 153401.

[10] T. Havermeier, T. Jahnke, K. Kreidi, R. Wallauer, S. Voss, M. Schöffler, S. Schössler, L. Foucar, N. Neumann, J. Titze, H. Sann, M. Kühnel, J. Voigtsberger, J. H. Morilla, W. Schöllkopf, H. Schmidt-Böcking, R. E. Grisenti, R. Dörner, *Phys. Rev. Lett.* **2010**, *104*, 133401.

[11] T. Ouchi, K. Sakai, H. Fukuzawa, X.-J. Liu, I. Higuchi, Y. Tamenori, K. Nagaya, H. Iwayama, M. Yao, D. Zhang, D. Ding, A. I. Kuleff, S. D. Stoychev, P. V. Demekhin, N. Saito, K. Ueda, *Phys. Rev. Lett.* **2011**, *107*, 053401.

[12] F. Trinter, J. B. Williams, M. Weller, M. Waitz, M. Pitzer, J. Voigtsberger, C. Schober, G. Kastirke, C. Müller, C. Goihl, P. Burzynski, F. Wiegandt, R. Wallauer, A. Kalinin, L. P. H. Schmidt, M. S. Schöffler, Y.-C. Chiang, K. Gokhberg, T. Jahnke, R. Dörner, *Phys. Rev. Lett.* **2013**, *111*, 233004.

[13] E. Kukk, T. D. Thomas, D. Céolin, S. Granroth, O. Travnikova, M. Berholts, T. Marchenko, R. Guillemin, L. Journel, I. Ismail, R. Püttner, M. N. Piancastelli, K. Ueda, M. Simon, *Phys. Rev. Lett.* **2018**, *121*, 073002.

[14] M. Kircher, J. Rist, F. Trinter, S. Grundmann, M. Waitz, N. Melzer, I. Vela-Perez, T. Mletzko, A. Pier, N. Strenger, J. Siebert, R. Janssen, V. Honkimäki, J. Drnec, P. V. Demekhin, L. P. H. Schmidt, M. S. Schöffler, T. Jahnke, R. Dörner, *Phys. Rev. Lett.* **2019**, *123*, 193001.

[15] B. Chen, H. Wang, Z. Wang, J. Han, A. B. S. Alquaity, H. Wang, N. Hansen, S. M. Sarathy, *Combust. Flame* **2019**, *202*, 208.

[16] N. S. Shuman, D. E. Hunton, A. A. Viggiano, *Chem. Rev.* **2015**, *115*, 4542.

[17] J.-K. Hsu, W.-H. Ip, *Planet. Sci. J.* **2021**, *2*, 160.

[18] T. P. Snow, V. M. Bierbaum, *Annu. Rev. Anal. Chem.* **2008**, *1*, 229.

[19] T. J. Millar, C. Walsh, T. A. Field, *Chem. Rev.* **2017**, *117*, 1765.

[20] J.-P. Mosnier, E. T. Kennedy, P. van Kampen, D. Cubaynes, S. Guilbaud, N. Sisourat, A. Puglisi, S. Carniato, J.-M. Bizau, *Phys. Rev. A* **2016**, *93*, 061401(R).

[21] S. Klumpp, A. A. Guda, K. Schubert, K. Mertens, J. Hellhund, A. Müller, S. Schippers, S. Bari, M. Martins, *Phys. Rev. A* **2018**, *97*, 033401.

[22] S. Bari, L. Inhester, K. Schubert, K. Mertens, J. O. Schunck, S. Dörner, S. Deinert, L. Schwob, S. Schippers, A. Müller, S. Klumpp, M. Martins, *Phys. Chem. Chem. Phys.* **2019**, *21*, 16505.

[23] K. Schubert, A. A. Guda, K. Mertens, J. O. Schunck, S. Schippers, A. Müller, S. Bari, S. Klumpp, M. Martins, *Phys. Chem. Chem. Phys.* **2019**, *21*, 25415.

[24] E. T. Kennedy, J. P. Mosnier, P. Van Kampen, J. M. Bizau, D. Cubaynes, S. Guilbaud, S. Carniato, A. Puglisi, N. Sisourat, *J. Phys. Conf. Ser.* **2019**, *1289*, 012003.

[25] R. Lindblad, L. Kjellsson, R. C. Couto, M. Timm, C. Bülow, V. Zamudio-Bayer, M. Lundberg, B. von Issendorff, J. T. Lau, S. L. Sorensen, V. Carravetta, H. Ågren, J.-E. Rubensson, *Phys. Rev. Lett.* **2020**, *124*, 203001.

[26] R. C. Couto, L. Kjellsson, H. Ågren, V. Carravetta, S. L. Sorensen, M. Kubin, C. Bülow, M. Timm, V. Zamudio-Bayer, B. von Issendorff, J. T. Lau, J. Söderström, J.-E. Rubensson, R. Lindblad, *Phys. Chem. Chem. Phys.* **2020**, *22*, 16215.

[27] S. Carniato, J.-M. Bizau, D. Cubaynes, E. T. Kennedy, S. Guilbaud, E. Sokell, B. McLaughlin, J.-P. Mosnier, *Atoms* **2020**, *8*, 67.

[28] M. Martins, S. Reinwardt, J. O. Schunck, J. Schwarz, K. Baev, A. Müller, T. Buhr, A. Perry-Sassmannshausen, S. Klumpp, S. Schippers, *J. Phys. Chem. Lett.* **2021**, *12*, 1390.

[29] R. Lindblad, L. Kjellsson, E. De Santis, V. Zamudio-Bayer, B. von Issendorff, S. L. Sorensen, J. T. Lau, W. Hua, V. Carravetta, J.-E. Rubensson, H. Ågren, R. C. Couto, *Phys. Rev. A* **2022**, *106*, 042814.

[30] J. Schwarz, F. Kielgast, I. Baev, S. Reinwardt, F. Trinter, S. Klumpp, A. Perry-Sassmannshausen, T. Buhr, S. Schippers, A. Müller, S. Bari, V. Mondes, R. Flesch, E. Rühl, M. Martins, *Phys. Chem. Chem. Phys.* **2022**, *24*, 23119.

[31] S. Leutwyler, J. P. Maier, L. Misev, *Chem. Phys. Lett.* **1982**, *91*, 206.

[32] U. Hefter, R. D. Mead, P. A. Schulz, W. C. Lineberger, *Phys. Rev. A* **1983**, *28*, 1429.

[33] R. D. Mead, U. Hefter, P. A. Schulz, W. C. Lineberger, *J. Chem. Phys.* **1985**, *82*, 1723.

[34] B. D. Rehfuss, D.-J. Liu, B. M. Dinelli, M.-F. Jagod, W. C. Ho, M. W. Crofton, T. Oka, *J. Chem. Phys.* **1988**, *89*, 129.

[35] K. M. Ervin, W. C. Lineberger, *J. Phys. Chem.* **1991**, *95*, 1167.

[36] H. B. Pedersen, C. Brink, L. H. Andersen, N. Bjerre, P. Hvelplund, D. Kella, H. Shen, *J. Chem. Phys.* **1998**, *109*, 5849.

[37] A. E. Bragg, R. Wester, A. V. Davis, A. Kammrath, D. M. Neumark, *Chem. Phys. Lett.* **2003**, *376*, 767.

[38] S. Iida, S. Kuma, H. Tanuma, T. Azuma, H. Shiromaru, *J. Phys. Chem. Lett.* **2020**, *11*, 10526.

[39] M. Iizawa, S. Kuma, N. Kimura, K. Chartkunchand, S. Harayama, T. Azuma, Y. Nakano, *J. Phys. Soc. Jpn.* **2022**, *91*, 084302.

[40] P. Yzombard, M. Hamamda, S. Gerber, M. Doser, D. Comparat, *Phys. Rev. Lett.* **2015**, *114*, 213001.

[41] M. Nötzold, R. Wild, C. Lochmann, R. Wester, *Phys. Rev. A* **2022**, *106*, 023111.

[42] R. C. Bilodeau, C. W. Walter, I. Dumitriu, N. D. Gibson, G. D. Ackerman, J. D. Bozek, B. S. Rude, R. Santra, L. S. Cederbaum, N. Berrah, *Chem. Phys. Lett.* **2006**, *426*, 237.

[43] B. A. Laws, S. T. Gibson, B. R. Lewis, R. W. Field, *Nat. Commun.* **2019**, *10*, 5199.

[44] N. Berrah, R. C. Bilodeau, I. Dumitriu, D. Toffoli, R. R. Lucchese, *J. Electron Spectrosc. Relat. Phenom.* **2011**, *183*, 64.

[45] N. Douguet, S. Fonseca dos Santos, T. N. Rescigno, *Phys. Rev. A* **2020**, *101*, 033411.

[46] S. Schippers, S. Ricz, T. Buhr, A. Borovik Jr, J. Hellhund, K. Holste, K. Huber, H.-J. Schäfer, D. Schury, S. Klumpp, K. Mertens, M. Martins, R. Flesch, G. Ulrich, E. Rühl, T. Jahnke, J. Lower, D. Metz, L. P. H. Schmidt, M. Schöffler, J. B. Williams, L. Glaser, F. Scholz, J. Seltmann, J. Viefhaus, A. Dorn, A. Wolf, J. Ullrich, A. Müller, *J. Phys. B* **2014**, *47*, 115602.

[47] A. Müller, D. Bernhardt, A. Borovik Jr, T. Buhr, J. Hellhund, K. Holste, A. L. D. Kilcoyne, S. Klumpp, M. Martins, S. Ricz, J. Seltmann, J. Viefhaus, S. Schippers, *Astrophys. J.* **2017**, *836*, 166.

[48] S. Schippers, T. Buhr, A. Borovik Jr, K. Holste, A. Perry-Sassmannshausen, K. Mertens, S. Reinwardt, M. Martins, S. Klumpp, K. Schubert, S. Bari, R. Beerwerth, S. Fritzsche, S. Ricz, J. Hellhund, A. Müller, *X-Ray Spectrom.* **2020**, *49*, 11.

[49] J. Viefhaus, F. Scholz, S. Deinert, L. Glaser, M. Ilchen, J. Seltmann, P. Walter, F. Siewert, *Nucl. Instrum. Methods Phys. Res. Sect. A* **2013**, *710*, 151.

[50] A. Perry-Sassmannshausen, T. Buhr, A. Borovik Jr, M. Martins, S. Reinwardt, S. Ricz, S.O. Stock, F. Trinter, A. Müller, S. Fritzsche, S. Schippers, *Phys. Rev. Lett.* **2020**, *124*, 083203.

[51] R. N. S. Sodhi, C. E. Brion, *J. Electron Spectrosc. Relat. Phenom.* **1984**, *34*, 363.

[52] A. Müller, E. Lindroth, S. Bari, A. Borovik Jr, P.-M. Hillenbrand, K. Holste, P. Indelicato, A. L. D. Kilcoyne, S. Klumpp, M. Martins, J. Viefhaus, P. Wilhelm, S. Schippers, *Phys. Rev. A* **2018**, *98*, 033416.

[53] F. Neese, F. Wennmohs, U. Becker, C. Riplinger, *J. Chem. Phys.* **2020**, *152*, 224108.

[54] F. Weigend, R. Ahlrichs, *Phys. Chem. Chem. Phys.* **2005**, *7*, 3297.

[55] F. Weigend, *Phys. Chem. Chem. Phys.* **2006**, *8*, 1057.

[56] K. Kaufmann, W. Baumeister, M. Jungen, *J. Phys. B* **1989**, *22*, 2223.

[57] T. Yanai, D. P. Tew, N. C. Handy, *Chem. Phys. Lett.* **2004**, *393*, 51.

[58] F. Neese, F. Wennmohs, A. Hansen, U. Becker, *Chem. Phys.* **2009**, *356*, 98.

[59] J. C. López V, A. L. Rivera, Y. F. Smirnov, A. Frank, *Int. J. Quantum Chem.* **2002**, *88*, 280.

[60] boost C^{++} libraries (version 1.7.5), [online]. available: https://www.boost.org.

[61] W. Shi, C. Li, H. Meng, J. Wei, L. Deng, C. Yang, *Comp. Theo. Chem.* **2016**, *1079*, 57.

[62] I. V. Hertel, C.-P. Schulz, Molecular Spectroscopy, in *Atoms, Molecules and Optical Physics 2: Molecules and Photons - Spectroscopy and Collisions*, Springer, Berlin, Heidelberg **2015**, chapter 5.6.6.

[63] A. Hansson, J. K. G. Watson, *J. Mol. Spectrosc.* **2005**, *233*, 169.

[64] P. Rosmus, H.-J. Werner, *J. Chem. Phys.* **1984**, *80*, 5085.

[65] T. X. Carroll, J. Hahne, T. D. Thomas, L. J. Sæthre, N. Berrah, J. Bozek, E. Kukk, *Phys. Rev. A* **2000**, *61*, 042503.

[66] M. Hoshino, K. Nakagawa, C. Makochekanwa, T. Tanaka, N. Kuze, M. Matsumoto, K. Fujiwara, A. De Fanis, Y. Tamenori, M. Kitajima, H. Tanaka, K. Ueda, *Chem. Phys. Lett.* **2006**, *421*, 256.

[67] D. Barret, A. Decourchelle, A. Fabian, M. Guainazzi, K. Nandra, R. Smith, J.-W. den Herder, *Astron. N.* **2020**, *341*, 224.

[68] M. Huang, C. Li, F. A. Evangelista, *J. Chem. Theory Comput.* **2022**, *18*, 219.